Chapter | twelve

Relative Measurements and Navigation

I roamed the infinite sky,
and soared in the ideal world,
and floated through the firmament.
But here I am, prisoner of measurement.

Khalil Gibran (1883–1931)

In this chapter, we discuss an application of both the EKF and UKF algorithms (discussed in Chapter 3) to the relative orbital navigation problem. The equations that relate Carrier-Phase Differential Global Positioning System (CDGPS) measurements to the relative state are the basis for the measurement models.

The relative state used in this chapter includes the quantities of interest for navigation and control, relative position and velocity of the vehicle, as well as several other quantities that are included in the augmented state so the filter will function properly. These other quantities, associated with the use of CDGPS, include the *clock offset*, the *clock drift rate*, and a *carrier-phase bias* for each GPS satellite that is tracked. The state vector used for relative navigation between two vehicles in this chapter is

$$\mathbf{x}_k = \begin{bmatrix} \boldsymbol{\rho}_{ij}(t_k) \\ \Delta b_{ij}(t_k) \\ \dot{\boldsymbol{\rho}}_{ij}(t_k) \\ \Delta \dot{b}_{ij}(t_k) \\ \Delta \beta_{ij}^{1} \\ \vdots \\ \Delta \beta_{ij}^{N} \end{bmatrix} = \begin{bmatrix} \textit{relative position vector} \\ \textit{clock offset} \\ \textit{relative velocity vector} \\ \textit{clock drift} \\ \textit{carrier phase bias, channel 1} \\ \vdots \\ \textit{carrier phase bias, channel N} \end{bmatrix} \tag{12.1}$$

where the relative vectors are expressed in the ECEF frame $\mathcal{F}$, discussed in Section 2.1. The relative position and velocity dynamics are defined by relations

Spacecraft Formation Flying; ISBN: 9780750685337

similar to the ones discussed in Chapter 4. The dynamical equations for the clock states for the carrier biases are shown in Section 12.1.

There are several methods for computing the relative position and velocity. The absolute states of the chief and deputy could be found and differenced. This has proven inadequate for close formations [43,183]. Another strategy, used here, calculates the relative state of the deputy vehicle, referenced to the position of the chief vehicle.

The absolute state is used in the process of obtaining GPS measurements and in functions external to navigation and control, so it is also estimated. There are many estimation techniques available to form an absolute state solution [42, 184,185]. The dynamics used for the absolute state estimation are presented here and are also used in the development of the relative dynamics equations.

12.1 DYNAMICAL MODELING

The two-body equations of motion in the ECI frame, Eq. (2.1), endowed with a thrust acceleration vector, $\mathbf{u}$, are given by

$$\ddot{\mathbf{r}} = -\frac{\mu \mathbf{r}}{\|\mathbf{r}\|^3} + \mathbf{u} \tag{12.2}$$

where the ECI position vector $\mathbf{r} = [\,X \quad Y \quad Z\,]^T$ has a magnitude of r.

The relative position and velocity terms in the state vector are governed by relative orbital dynamics equations, which can be derived from the absolute orbital dynamics equations, as discussed in Chapter 4. The relative position vector, $\boldsymbol{\rho}_{ij}$, is defined as the difference between the absolute position vectors of vehicles i and j,

$$\boldsymbol{\rho}_{ij} = \mathbf{r}_j - \mathbf{r}_i \tag{12.3}$$

It follows that the relative acceleration is defined by the difference of the two absolute accelerations, with thrust accelerations accounted for with the term $\Delta\mathbf{u}_{ij}$,

$$\ddot{\boldsymbol{\rho}}_{ij} = \ddot{\mathbf{r}}_j - \ddot{\mathbf{r}}_i + \Delta\mathbf{u}_{ij} \tag{12.4}$$

By using the two-body relation (12.2), one can obtain an expression for the relative dynamics in the ECI frame. However, the GPS constellation and the GPS navigation message use the ECEF reference frame, so ECEF is a natural reference frame for navigation filters using GPS measurements. To transform from the ECI frame to the ECEF frame, a correction term accounting for the Coriolis effect is added to the dynamics equation:

$$\ddot{\boldsymbol{\rho}}_{ij} = \frac{\mu}{\|\mathbf{r}_i\|^3}\left[\mathbf{r}_i - \frac{\|\mathbf{r}_i\|^3(\mathbf{r}_i + \boldsymbol{\rho}_{ij})}{\sqrt{(\|\mathbf{r}_i\|^2 + 2\mathbf{r}_i \cdot \boldsymbol{\rho}_{ij} + \|\boldsymbol{\rho}_{ij}\|^2)^3}}\right] + \Delta\mathbf{u}_{ij} + \mathbf{C}_{ECEF} \tag{12.5}$$

where the differential perturbations have been added, and

$$\mathbf{C}_{ECEF} = 2\boldsymbol{\Omega}_e \times \dot{\boldsymbol{\rho}}_{ij} + \boldsymbol{\Omega}_e \times (\boldsymbol{\Omega}_e \times \boldsymbol{\rho}_{ij}) \tag{12.6}$$

where $\boldsymbol{\Omega}_e \equiv {}^{\mathscr{I}}\boldsymbol{\Omega}^{\mathscr{F}} = [0, 0, \Omega_e]^T$ is the angular velocity vector of the ECEF frame relative to the ECI frame, so that $\Omega_e = 7.292 \times 10^{-5}$ rad/s is the rotation rate of the Earth about its axis. Other, more sophisticated, methods for performing the ECI to ECEF rotation are described in Ref. [12], but the propagation time in the Kalman filter is typically very short, so Eq. (12.6) is usually sufficient.

The Jacobian F of the nonlinear relative dynamics in Eq. (12.5) is required for the linear state propagation scheme and for the covariance propagation. The linear dynamics matrix for the position and velocity states is given as

$$F = \begin{bmatrix} F_{pp} & F_{pv} \\ F_{vp} & F_{vv} \end{bmatrix} \tag{12.7}$$

where the position and velocity partitions are

$$F_{pp} = 0_{3\times 3} \tag{12.8}$$

$$F_{pv} = I_3 \tag{12.9}$$

$$F_{vp} = \frac{\mu}{r^3}\begin{bmatrix} -1 + 3\dfrac{X^2}{r^2} - \dfrac{r^3}{\mu}\Omega_e^2 & 3\dfrac{XY}{r^2} & 3\dfrac{XZ}{r^2} \\ 3\dfrac{YX}{r^2} & -1 + 3\dfrac{Y^2}{r^2} - \dfrac{r^3}{\mu}\Omega_e^2 & 3\dfrac{YZ}{r^2} \\ 3\dfrac{ZX}{r^2} & 3\dfrac{ZY}{r^2} & -1 + 3\dfrac{Z^2}{r^2} \end{bmatrix} \tag{12.10}$$

$$F_{vv} = \begin{bmatrix} 0 & 2\Omega_e & 0 \\ -2\Omega_e & 0 & 0 \\ 0 & 0 & 0 \end{bmatrix} \tag{12.11}$$

CDGPS navigation techniques require that time be known with a high degree of accuracy. The clocks on the local receivers are relatively low-quality and unstable, so a clock offset and a clock drift rate must be estimated by including each in the Kalman filter state definition. The dynamics of the clock offset from GPS time, b, and the clock drift rate, $\dot{b}$, are modeled as

$$\begin{bmatrix} \dot{b} \\ \ddot{b} \end{bmatrix} = \begin{bmatrix} 0 & 1 \\ 0 & 0 \end{bmatrix}\begin{bmatrix} b \\ \dot{b} \end{bmatrix} + \begin{bmatrix} 0 \\ 1 \end{bmatrix} w_b \tag{12.12}$$

When the single differences are performed between two vehicles, the relative clock dynamics retain only the differential white noise term,

$$\begin{bmatrix} \Delta\dot{b}_{ij} \\ \Delta\ddot{b}_{ij} \end{bmatrix} = \begin{bmatrix} 0 & 1 \\ 0 & 0 \end{bmatrix}\begin{bmatrix} \Delta b_{ij} \\ \Delta\dot{b}_{ij} \end{bmatrix} + \begin{bmatrix} 0 \\ 1 \end{bmatrix} w_{\Delta b} \tag{12.13}$$

Thus, in the state propagation step, the clock model will contribute nothing to the state transition matrix, but will introduce terms in the noise covariance model.

Each GPS carrier phase measurement includes a bias term. This bias is treated as a constant that must be estimated. A description of the carrier bias is found in Section 12.2. The differential biases are modeled as constants,

$$\Delta\dot{\beta}_{ij}^{m} = 0 \tag{12.14}$$

To summarize, the full relative state is defined as

$$\mathbf{x}_k = \begin{bmatrix} \boldsymbol{\rho}_{ij}(t_k) \\ \Delta b_{ij}(t_k) \\ \dot{\boldsymbol{\rho}}_{ij}(t_k) \\ \Delta\dot{b}_{ij}(t_k) \\ \Delta\beta_{ij}^{1} \\ \vdots \\ \Delta\beta_{ij}^{N} \end{bmatrix} \tag{12.15}$$

The carrier biases, $\Delta\beta_{ij}^{m}$, are constant and are ignored during the state propagation step. A truncated vector, which excludes the biases $\Delta\beta_{ij}^{1}, \ldots, \Delta\beta_{ij}^{N}$, is propagated. The linearized dynamics of the position, velocity, and clock states are modeled as

$$\dot{\mathbf{x}}(t) = \begin{bmatrix} F_{pp} & 0 & F_{pv} & 0 \\ 0 & 0 & 0 & 1 \\ F_{vp} & 0 & F_{vv} & 0 \\ 0 & 0 & 0 & 0 \end{bmatrix} \mathbf{x}(t) + \mathbf{w} + \mathbf{u} \tag{12.16}$$

where

$$\mathbf{w} = \begin{bmatrix} \mathbf{0}_{1\times 4} & \mathbf{w}_{\boldsymbol{\rho}} & w_{\Delta b} \end{bmatrix}^T \tag{12.17}$$

$$\mathbf{u} = \begin{bmatrix} \mathbf{0}_{1\times 4} & \Delta\mathbf{u}_{ij} & 0 \end{bmatrix}^T \tag{12.18}$$

The dynamics and process noise models are then discretized as discussed in Section 3.8.

12.2 MEASUREMENT UPDATE: CARRIER-PHASE DIFFERENTIAL GPS

The code-based pseudorange is used to calculate the absolute state. The code phase, χ, is

$$\chi_i^m = \|\mathbf{r}^{m_i} - \mathbf{r}_i\| + b_i + B^{m_i} + I_i^m + v_\chi \tag{12.19}$$

where $\|\mathbf{r}^{m_i} - \mathbf{r}_i\|$ represents the true range between where the vehicle i is at the measurement time and the GPS satellite m at the transmission time. Offset errors in the clock of vehicle i and the GPS satellite m are captured in the terms b_i and B^{m_i}. The unmodeled (and unknowable) phenomena that affect the code phase measurement are included in the noise term, ν_χ. The term I_i^m models the delay imposed on the signal by the ionosphere. This term is modeled as

$$I_i^m = \frac{82.1 \times TEC}{F_c^2 \times \sqrt{\sin^2 \gamma_i^m + 0.076} + \sin \gamma_i^m} \tag{12.20}$$

where TEC is the total electron count in the atmosphere, a varying quantity influenced by, among other things, local solar illumination and sunspot activity. The signal frequency F_c, and the elevation angle of the GPS satellite m with respect to vehicle i, γ_i^m, both influence the path delay caused by the ionosphere.

The carrier phase pseudorange, similarly relating range, clock states, and ionospheric delay, is

$$\phi_i^m = \|\mathbf{r}^{m_i} - \mathbf{r}_i\| + b_i + B^{m_i} + \beta_i^m - I_i^m + \nu_\phi \tag{12.21}$$

A carrier phase noise term, ν_ϕ in Eq. (12.21), replaces the code noise from Eq. (12.19). The difference in the effect of wave delay seen by the carrier and group delay seen by the code is reflected in the carrier pseudorange in Eq. (12.21) that has an ionospheric delay term that is opposite in sign.

The additional term β_i^m introduced in the carrier pseudorange is a carrier phase bias. The bias is required to deal with an integer ambiguity in the phase measurement. The distance between the GPS satellite and the vehicle can be expressed as the sum of the carrier phase ϕ, and an integer multiple k of the carrier wavelength λ,

$$d = \phi + k\lambda$$

where $\lambda \approx 19.2$ cm. The distance viewed as being measured in units of carrier wavelengths, the fractional part of the distance, which is the carrier phase measurement, is known very accurately. The part of the distance that is covered by the integer multiple of wavelengths cannot be determined immediately from the information in the carrier phase measurement. Fortunately, there are a number of techniques available to determine this integer number. We will use a passive technique called *kinematic positioning*. As the GPS constellation and the spacecraft move relative to each other, the range measurements will change, but the bias remains constant [43]. With measurements collected over time, the biases are then observable and can be estimated. While this technique results in a longer startup time, it is quite simple and the biases do not change after the initial startup period. When new GPS satellites enter the antenna's field of

view, the biases in their measurements can be determined very quickly. Another advantage to this approach is that because the bias estimates are not necessarily required to be integers, the bias estimate can include constant errors, such as those potentially introduced by an antenna line bias or the correlator inside the receiver.

The line-of-sight (LOS) vector is a unit vector whose origin is vehicle i and points towards GPS satellite m,

$$\mathbf{los}_i^m = \frac{\mathbf{r}^{m_i} - \mathbf{r}_i}{\|\mathbf{r}^{m_i} - \mathbf{r}^i\|} \tag{12.22}$$

The vectors in the LOS equation refer to the positions of vehicle i at the time of measurement and the GPS satellite m at the time of signal transmission. The measurement matrix H includes the LOS vectors for each GPS satellite tracked,

$$H_{\mathbf{LOS}} = \begin{bmatrix} \mathbf{los}_i^1 \\ \vdots \\ \mathbf{los}_i^N \end{bmatrix} \tag{12.23}$$

The Geometric Dilution of Precision (GDOP), indicates the distribution of satellites,

$$\text{GDOP} = \sqrt{\text{trace}\,[(H_{\mathbf{LOS}}^T H_{\mathbf{LOS}})^{-1}]} \tag{12.24}$$

A low GDOP indicates good GPS satellite coverage, which means that measurements are available in all directions, providing good observability of the state. Conversely, a large GDOP indicates poor coverage and may result in degraded estimates.

When two vehicles in close proximity track the same GPS satellites, the measurement for GPS satellite m taken by vehicle i will see many of the same errors as the measurement taken by vehicle j. If these measurements are differenced, then the errors cancel to a large degree. This is the crux of the advantage of CDGPS. The carrier differential phase is defined as

$$\Delta\phi_{ij}^m = \phi_j^m - \phi_i^m \tag{12.25}$$

where ϕ_i^m and ϕ_j^m are the raw carrier phases from GPS satellite m measured by vehicles i and j. This difference is formed for each GPS satellite commonly tracked by both vehicles. Substituting the Eq. (12.21) into this difference yields an expression for the carrier differential phase measurement,

$$\begin{aligned} \Delta\phi_{ij}^m = {} & \|\mathbf{r}^{m_i} - \mathbf{r}_i\| - \|\mathbf{r}^{m_j} - \mathbf{r}_j\| + \Delta\beta_{ij}^m \\ & + \Delta b_{ij} + \Delta B_{ij}^m + \Delta I_{ij}^m + \nu_{\Delta\phi} \end{aligned} \tag{12.26}$$

The carrier differential phase can be expressed explicitly as a function of the relative state, as defined in Eq. (12.3),

$$\begin{aligned}\Delta\phi_{ij}^{m} = &\|\mathbf{r}^{m_i} - \mathbf{r}_i\| - \|\mathbf{r}^{m_j} - (\mathbf{r}_i + \boldsymbol{\rho}_{ij})\| + \Delta\beta_{ij}^{m} \\ &+ \Delta b_{ij} + \Delta B_{ij}^{m} + \Delta I_{ij}^{m} + \nu_{\Delta\phi}\end{aligned} \tag{12.27}$$

As in the equations for relative orbital mechanics, the relative carrier phase measurement equation retains the absolute state of the reference vehicle. Also, the error terms introduced for the raw carrier phase measurements have become differential terms. If the vehicles are close, it is reasonable to assume that the terms modeling the GPS satellite clock error and the ionospheric delay cancel,

$$\Delta\phi_{ij}^{m} = \|\mathbf{r}^{m_i} - \mathbf{r}_i\| - \|\mathbf{r}^{m_j} - (\mathbf{r}_i + \boldsymbol{\rho}_{ij})\| + \Delta\beta_{ij}^{m} + \Delta b_{ij} + \nu_{\Delta\phi} \tag{12.28}$$

In summary, the measurement vector, $\mathbf{y}$, contains all the measurements that are used in the Kalman filter. The GPS receiver used herein tracks up to 12 GPS satellites, so the measurement vector

$$\mathbf{y}_k = \begin{bmatrix} \Delta\phi_{ij}^{1}(t_k) \\ \vdots \\ \Delta\phi_{ij}^{N}(t_k) \end{bmatrix} \tag{12.29}$$

may include as many as $N = 12$ differential carrier phase measurements. Given an estimate of the relative state, the nonlinear measurement equation is

$$\begin{aligned}\hat{\mathbf{y}}_k = &\begin{bmatrix} \|\hat{\mathbf{r}}^{1_i} - \hat{\mathbf{r}}_i\| - \|\hat{\mathbf{r}}^{1_j} - (\hat{\mathbf{r}}_i + \boldsymbol{\rho}_{ij})\| + \Delta b_{ij} + \Delta\beta_{ij}^{1} + \Delta\hat{B}_{ij}^{1} \\ \vdots \\ \|\hat{\mathbf{r}}^{N_i} - \hat{\mathbf{r}}_i\| - \|\hat{\mathbf{r}}^{N_j} - (\hat{\mathbf{r}}_i + \boldsymbol{\rho}_{ij})\| + \Delta b_{ij} + \Delta\beta_{ij}^{N} + \Delta\hat{B}_{ij}^{N} \end{bmatrix} \\ &+ \begin{bmatrix} \Delta\hat{I}_{ij}^{1}(\hat{\mathbf{r}}_i, \hat{\boldsymbol{\rho}}_{ij}, \hat{\mathbf{r}}^{m}) + \nu_{\Delta\phi} \\ \vdots \\ \Delta\hat{I}_{ij}^{N}(\hat{\mathbf{r}}_i, \hat{\boldsymbol{\rho}}_{ij}, \hat{\mathbf{r}}^{m}) + \nu_{\Delta\phi} \end{bmatrix} = \hat{h}_k(\hat{\mathbf{x}}_k^{-}) + \nu\end{aligned} \tag{12.30}$$

and the associated Jacobian is

$$H_k = \begin{bmatrix} H_{\mathbf{LOS}(N\times 3)} & \mathbf{1}_{N\times 1} & 0_{N\times 3} & \mathbf{0}_{N\times 1} & I_N \end{bmatrix} \tag{12.31}$$

12.3 COMPARISON OF EKF AND UKF FOR RELATIVE NAVIGATION

The purpose of this section is to investigate whether the UKF may improve the relative navigation for formation flying spacecraft, particularly when vehicle separations exceed 1 km. Tests are performed with simulated measurements to show that there is little performance difference between the two forms of the UKF discussed in Chapter 3 for this application. These simulations also show

Table 12.1 Comparison of the standard additive and square root forms of the UKF

	Position (m)	Velocity (m)
Mean, $\mu_{UKF-S} - \mu_{UKF-A}$	3.8277e-005	4.5264e-008
Standard deviation, $\sigma_{UKF-S} - \sigma_{UKF-A}$	1.2474e-005	3.0500e-008

that the additive form of the UKF, described in Subsection 3.9.2, requires much less computation.

We performed a set of simulations to compare the performance of the UKF to the performance of the EKF. Simulations used data generated with orbits calculated in `FreeFlyer`^{TM} and using stored GPS receiver measurements compared to truth data from experiments at NASA Goddard Space Flight Center (GSFC). The results of these simulations confirm that the UKF outperforms EKF when the separation between vehicles is greater than 1 km or the discrete time step of the filter is greater than 10–15 seconds.

The UKF-S has the potential for improved performance and numerical stability, but these improvements are not guaranteed, so both the Additive and Square Root form of the UKF (UKF-A and UKF-S) were implemented and compared. Since the UKF was designed to better handle the nonlinearities, a 10 km baseline (BL) example was used for this comparison. The estimator was given simulated measurements that were created from stored absolute trajectories. White noise was applied to the dynamics and the measurements. The performance was seen to vary when the filter was run for different randomly generated measurement noise sequences. Twenty different random measurement noise profiles were generated and stored, and the simulation was run for each profile. The average of the results from 20 profiles provided a better basis for evaluating the filter than the results from any single noise profile. Because nonlinearities in the dynamics may have more of an effect when the filter has a longer time step, the UKF-A and UKF-S were compared for time steps between 5 and 60 seconds.

Figure 12.1 shows the differences in the means and standard deviations for the position and velocity estimates from the UKF-A and UKF-S. The results for the individual runs are shown in the background in gray, and the mean over all the noise profiles is shown in a strong black line. The differences for any single run are very small, and, when averaged over the 20 noise profiles, the difference is negligible. Also, the mean differences do not grow or shrink significantly as the time step is increased. The results, summarized in Table 12.1, indicate that there is no performance advantage to using the UKF-S in relative navigation filters. Because there is no significant performance difference, and the UKF-A is easier to implement, it was the one used for comparisons of the UKF and EKF.

Since the UKF was developed to better handle nonlinear dynamics and measurements, it is expected that the UKF will perform better than the EKF only when the nonlinearities become significant. The errors associated with

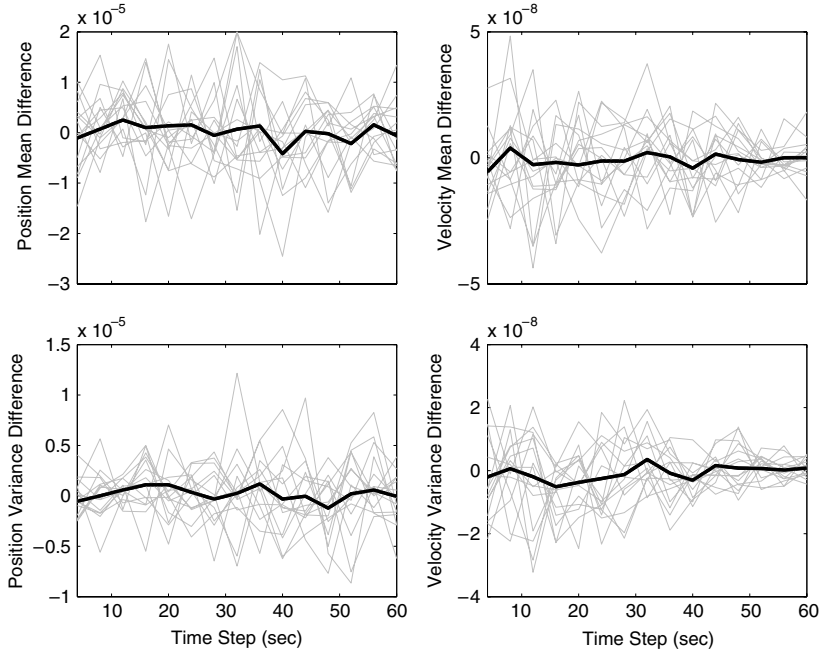

FIGURE 12.1 Negligible performance difference between UKF-A and UKF-S.

nonlinearities are expected to increase as the baseline distance between the two vehicles grows and as the filter time step increases.

Several sets of simulations were created to explore the performance differences in the EKF and UKF. To observe the effects of both increased baseline and time step, the simulations were conducted for baselines of 100 m, 1 km, and 10 km for time steps between 5 seconds and 1 minute. Comparisons were repeated in both a simulated environment and a more realistic environment created using stored data from GSFC. The two environments have different advantages. The total simulation environment provides control over every variable, from noise levels, to perturbations, to satellite coverage. However, simulation results are usually required to be corroborated by data from real hardware. For this reason, simulations based on `FreeFlyer`™ trajectories and simulations based on recorded hardware experiments at GSFC are used. A summary of these environments is given below.

- **`FreeFlyer`™-based simulations** The original `MATLAB`® simulation trajectories were created with a simple propagator. Perturbations and other real-world effects were coarsely simulated by adding white noise into the dynamics propagation. This is exactly the dynamics model used in the EKF and the UKF. The simulation is more realistic if it uses truth trajectories created with a dynamics model that has a much higher fidelity than the model used in the filter. The `FreeFlyer`™ commercial orbital dynamics simulation

Table 12.2 Summary of the simulations and results

Baseline	FreeFlyer™ data	GSFC data
100 m	Fig. 12.2	Fig. 12.5
1 km	Fig. 12.3	Fig. 12.6
10 km	Fig. 12.4	Fig. 12.7

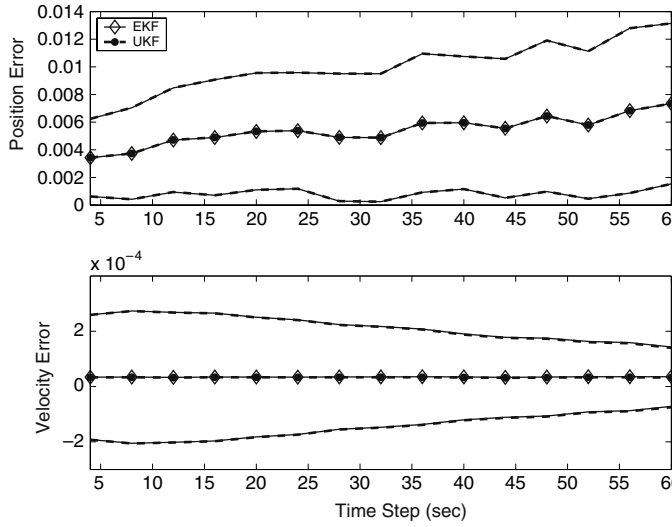

FIGURE 12.2 FreeFlyer™, BL = 100 m.

software can create very high fidelity trajectories that include perturbation forces including higher-order gravity terms, solar radiation pressure, third body gravity effects, and aerodynamic forces [186]. For the EKF/UKF comparison, FreeFlyer™ was used to create the truth trajectories from which the simulated measurements were derived. Each simulation was repeated for 20 stored noise profiles and the results were averaged.

- **GSFC stored-data simulations** The GSFC Formation Flying Testbed has a Spirent simulator that models vehicle motion and the GPS satellite constellation and creates an RF signal that mimics the input of the vehicle antenna in space. The Spirent trajectories can be stored as truth data and the output of the GPS receiver is stored to provide future measurement inputs to the filter. The truth and measurements can be post-processed to evaluate various estimators.

A summary of the simulations used to compare the EKF and UKF is shown in Table 12.2. The results of the comparisons are shown in Figs. 12.2–12.7. Each figure has subplots for position and velocity. The mean of the estimate error and bounds for the standard deviation of the error are shown

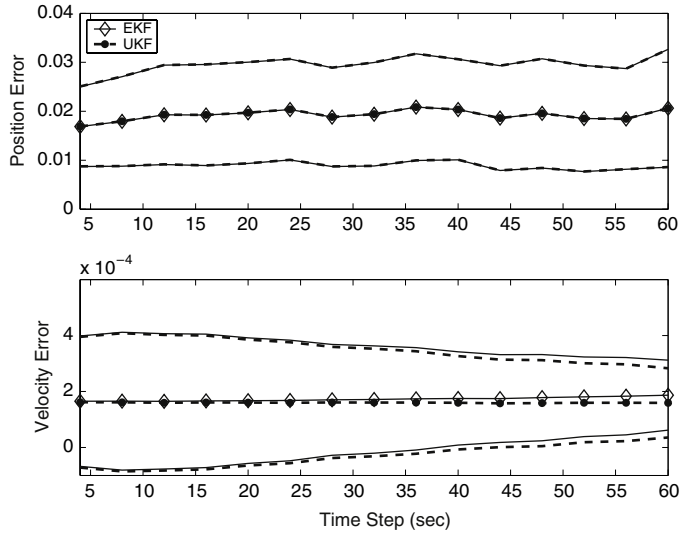

FIGURE 12.3 FreeFlyer™, BL = 1 km.

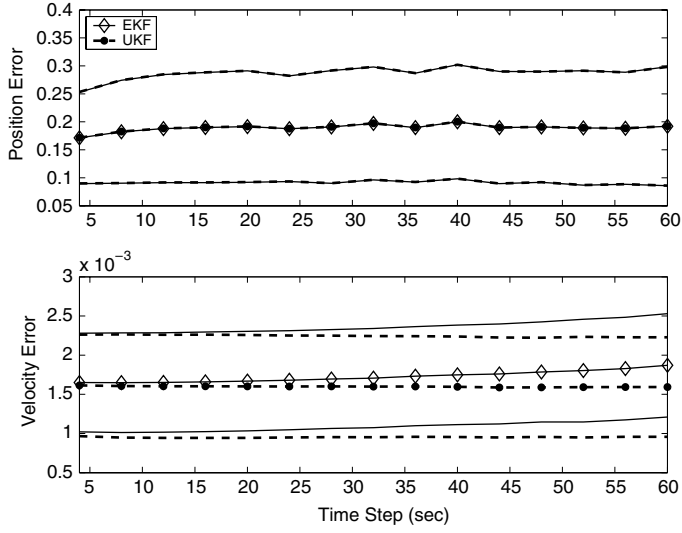

FIGURE 12.4 FreeFlyer™, BL = 10 km.

for both the EKF and UKF. The errors are shown against an axis, indicating the discrete time step of the filter. These six plots contain a large amount of information, and will be used to demonstrate several trends. The set of figures will be discussed (i) as individual entities; (ii) across a set of baseline distances, evaluating FreeFlyer™ and GSFC results separately; and (iii) between FreeFlyer™ and GSFC results, evaluating each baseline distance separately. Prior to initiating a detailed discussion of the results, a summary of

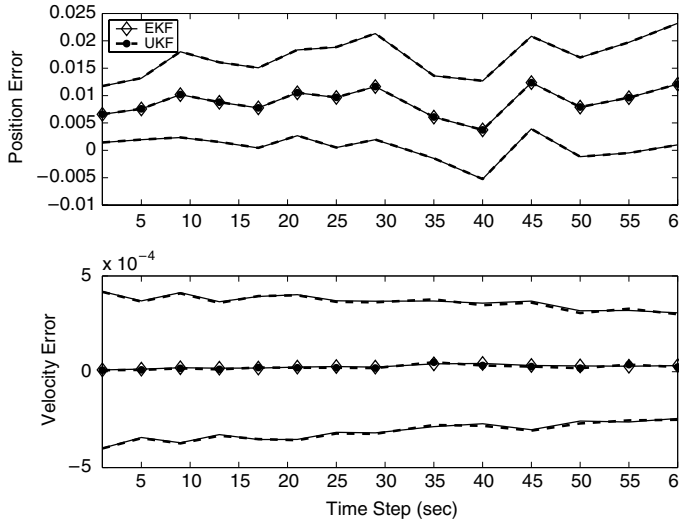

FIGURE 12.5 GSFC, BL = 100 m.

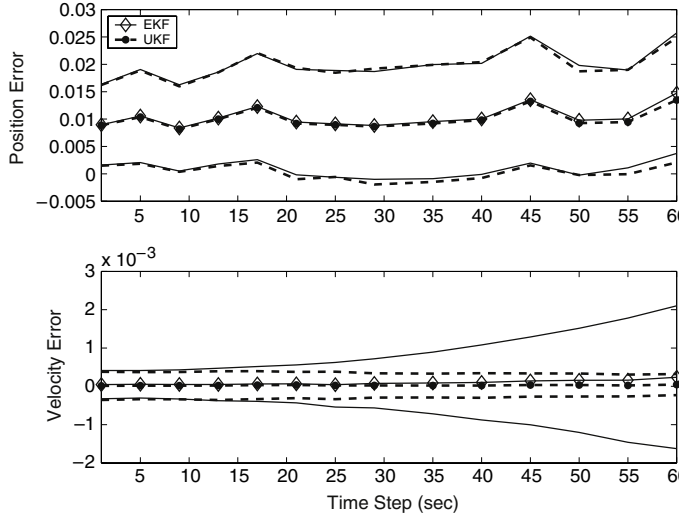

FIGURE 12.6 GSFC, BL = 1 km.

the questions addressed is listed below.

1. **Examining a single figure**
   - How do the errors for the EKF and UKF results compare?
   - Do the means grow as the time step is increased?
   - Do the standard deviations grow as the time step is increased?
   - Does the time step increase have a greater effect on position or velocity estimates?

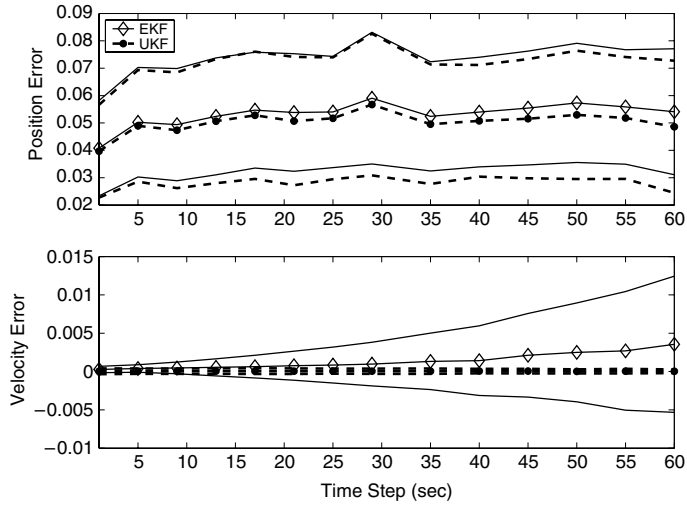

FIGURE 12.7 GSFC, BL = 10 km.

2. **Comparing plots across 3 baselines for same environment**
   - How do the mean values change across the 3 baselines?
   - Do the standard deviations increase across the 3 baselines?
   - If the standard deviation increases with time step for one baseline, does it in the others? If not, is there a reasonable explanation?
   - Does changing the baseline affect the position and velocity differently?
3. **Comparing `FreeFlyer`™ GSFC plots for same baselines**
   The results from the `FreeFlyer`™ and GSFC simulations are not expected to agree numerically. The `FreeFlyer`™ based simulations provide much more control over the truth trajectories and perturbation effects. The measurements are created by adding white noise to the output of equations. This model was also used in the estimator. At GSFC, the real `Orion`™ hardware with the many associated uncertainties, was used to create the measurements. For example, thermal variation has been known to affect the measurements. Clock uncertainties, poor electrical connections, or unexpected interference might also contribute errors. In general, the simulated measurements produce better estimates. However, trends seen in simulation are also found in hardware tests, so both are used in the comparisons.
   - When the trends in the `FreeFlyer`™ and GSFC simulations are similar, how do the `FreeFlyer`™ results reinforce interpretation for GSFC performance?
   - When the trends are different, do simulation differences provide a reasonable explanation?

- Finally, do the FreeFlyer™ and GSFC provide the same answer for the question of when does the UKF performs better?

Several expectations about the performance of the EKF and UKF and about the results of FreeFlyer™ and GSFC simulations are also useful to consider before proceeding.

- The UKF should perform better when the dynamics model breaks down. The dynamics model breaks down when the time step or baseline distance increases significantly.
- Dynamics models in both the EKF and UKF are more similar to the model that created the FreeFlyer™ trajectory. Since the velocity estimate depends on the quality of the velocity model, FreeFlyer™ simulations may perform better for velocity estimates.
- The filter measurement models closely match those used to create measurements from the FreeFlyer™ simulated trajectory. The hardware used to record GSFC measurements may or may not reflect the measurement model in the filter. This suggests FreeFlyer™ simulations may perform better.

Though results are shown for both position and velocity estimates, the velocity performance is much more important. The error in the velocity estimate has more effect on the knowledge of semimajor axis error than does the error in position. Since the semimajor axis error influences closed-loop control performance, and the navigation system exists primarily to aid in the control system, the velocity performance will be used as the final discriminator between the EKF and UKF.

12.3.1 Comparison for single baseline, as time step increases

Each of the six figures shows the mean and the 1σ bounds around the mean for position and velocity errors. The individual figures are useful in evaluating whether there is an advantage in using the UKF for a particular scenario. For example, at 100 m, the position and velocity means are nearly identical for the UKF and EKF. The standard deviation increases very slightly with the time step. In general, the nonlinearities at 100 m, even at a longer time step, are not significant enough to warrant using a UKF. At 1 km and 10 km, the velocity means are higher for the EKF, and the velocity standard deviations diverge as the time step increases. In these cases, the UKF would be a better choice.

12.3.2 Comparison as baselines increase

Figures 12.2–12.7 show that as the baseline is increased, the mean values for position and velocity errors also increase. This degradation of estimation accuracy concurs with results reported in Ref. [43]. When the nonlinear equations were linearized, the higher-order terms of the series expansion are truncated.

The linearization error increases with the distance between vehicles. The truncation is accounted for in the filter by including it in the process noise term. The process noise must therefore be increased as the baseline (and the corresponding truncation error) is increased. The results of this increase in process noise are increases in the position and velocity errors. Similarly, as the baseline grows, the standard deviation trends change from being tapered or constant as the time step increases, to diverging with time step increases.

Though the errors grow with the baseline size, the UKF still offers advantages over the EKF. This is seen in the velocity performance of the UKF, particularly in Figs. 12.6 and 12.7. Interesting differences in the velocity standard deviation of the FreeFlyer™ and GSFC simulations arise and are discussed in the following subsubsection.

12.3.3 Comparison for FreeFlyer™ and GSFC simulations

As stated before, the results from FreeFlyer™ and GSFC simulations are not expected to agree numerically. The 100 m baseline case was unremarkable: the EKF and UKF produced nearly identical results, with position means and standard deviations both showing slight increases in the FreeFlyer™ and GSFC simulations. The velocity means were constant for both simulation environments. The velocity standard deviation bounds became smaller, though this effect was more subtle for the GSFC simulations.

With 1 km baselines, the position trends are similar in the FreeFlyer™ and GSFC simulations. The mean values increase slightly with time step, and the standard deviation bounds flare slightly at the largest time steps. There is no significant difference in EKF and UKF performance in position estimation. As in the 100 m baseline simulations, the mean of velocity errors show little growth as the time step increases. The velocity mean of the EKF is slightly higher than the UKF mean for the largest time steps.

An interesting difference is seen in the standard deviations of velocity error produced by the FreeFlyer™ and GSFC simulations, at a 1 km baseline. In the FreeFlyer™ simulations, the standard deviations for both the EKF and the UKF decrease as the time step increases. In the GSFC simulations, the UKF velocity standard deviation shows a slight decrease as well. However, this is nearly obscured by the dramatic *increase* in the EKF velocity standard deviation. The question is why the EKF velocity diverges in GSFC simulations and not in the FreeFlyer™ simulations. The dynamics model in the filter is a simple two-body model with J_2 perturbations. This is closer to the model used to create the FreeFlyer™ trajectory than it is to the model that governs the GSFC dynamics. FreeFlyer™ corresponds to a case that is in between "perfectly modeled dynamics" and "fully realistic dynamics". Since the velocity estimates strongly depend on the quality of the dynamics model, it is reasonable to expect that the GSFC simulations will show poor performance for combinations of the separation and time step that are shorter than for the FreeFlyer™ simulations. In addition, the "measurements" used in the FreeFlyer™ simulations were

created with the measurement equation, while those used in the GSFC simulations were recorded with real hardware. Accordingly, FreeFlyer™ simulations also fall somewhere between "perfectly modeled measurements" and "fully realistic measurements".

This difference in velocity standard deviation behavior in FreeFlyer™ and GSFC simulations continues in the 10 km baseline examples. In the GSFC simulations, in Fig. 12.7, the EKF velocity mean becomes much larger than the UKF velocity mean at large time steps exceeding even the UKF 1σ bounds. The EKF is so much worse in this case that the UKF mean and standard deviation lines appear on top of each other – the EKF velocity standard deviation bounds diverge fairly explosively. Overall, the errors in the EKF velocity at 10 km eclipse the UKF errors. In comparison, while the FreeFlyer™ simulations show the UKF errors are smaller than the EKF errors, the difference is not as dramatic. This is attributed to the differences in the FreeFlyer™ and GSFC simulation setups.

Also of significance, in the 1 km FreeFlyer™ simulations, the velocity standard deviations decreased for the larger time steps, in Fig. 12.3. Conversely, they appear nearly constant in the 10 km FreeFlyer™ simulations, in Fig. 12.4. This suggests the FreeFlyer™ simulations will follow a trend seen in the 100 m and 1 km GSFC simulations, where the velocity standard deviation *decreased* for the larger time steps in the former, but *increased* for larger time steps in the latter. The trend appears more gradually in the FreeFlyer™ simulations than it did in the GSFC simulations, where the EKF velocity standard deviations failed dramatically when the distance was increased from 100 m to 1 km. Still, it appears that the dynamics model is beginning to fail even in the FreeFlyer™ simulations. This trend is affirmed for the FreeFlyer™ model in a final simulation with extreme nonlinearities, in Subsection 12.3.4, where the EKF mean and standard deviations diverge with the sharpness seen in the GSFC simulations.

Overall, the UKF performs better than the EKF when the baseline distance and time step are both increased. This assessment is based on the smaller means and standard deviation bounds of the velocity errors, which is the parameter that most strongly influences closed-loop control performance. The advantage of the UKF is especially apparent in GSFC simulations, whose dynamics and measurements are more realistic than the FreeFlyer™ simulations.

12.3.4 A final example

The previous discussion presented examples that showed the UKF outperforming the EKF as the baselines and time steps increased. This confirmed the hypothesis that the UKF, designed to better handle nonlinearities in the dynamics and measurement models, would become advantageous when the system nonlinearities are accentuated.

A final example with an extremely long baseline of 100 km is presented in Fig. 12.8. The nonlinearities are especially insidious here, as the CW equations fail rapidly at this large separation. Also, at this distance, the ionospheric effects

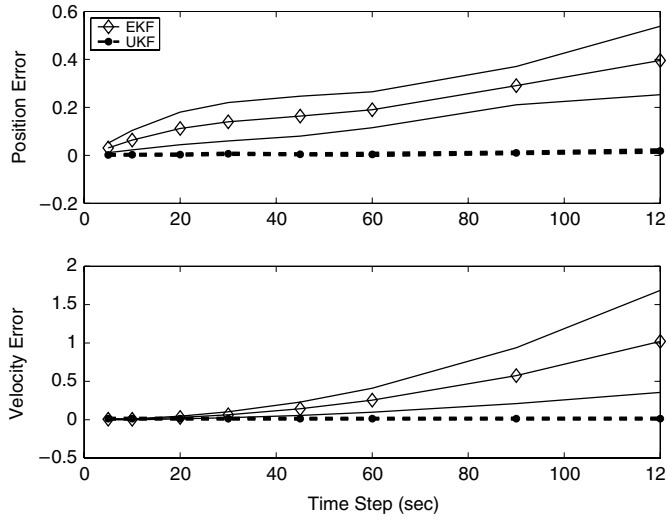

FIGURE 12.8 FreeFlyer™, baseline 100 km.

would begin to dominate [187]. At very small time steps, the EKF and UKF performance is comparable. This is because the estimate is corrected very frequently with new measurements. At higher time steps, the filter depends on the dynamics model to propagate between states, but when the dynamics model is poor, the propagated state error grows rapidly. If this error is not corrected quickly, then the filter will diverge. The UKF uses the nonlinear dynamics and measurement equations and employs a much better method of propagating the state error covariance. As a result, the performance is more consistent at longer baselines and longer time steps, and the UKF does not diverge, which is in stark contrast to the EKF results in Fig. 12.8.

This example underscores the potential for the UKF in situations when nonlinearities, including those caused by long time steps or large separations, are particularly important. Long time separations and eccentric orbits are likely to be required of some future missions and could reasonably benefit from the UKF.

SUMMARY

We discussed relative measurements and relative navigation using CDGPS, and compared the estimation of spacecraft relative states using EKF and UKF. Overall, the UKF performs better than the EKF for larger separations and longer time steps. This assessment is based on the smaller mean values and standard deviation bounds of the velocity errors, which is the parameter that most strongly influences closed-loop control performance. The advantage of the UKF is especially apparent in the GSFC simulations, which represent a more realistic setup (in particular the measurements) than the FreeFlyer™ simulations.